Journal of Materials Chemistry C

ROYAL SOCIETY OF CHEMISTRY

PAPER

View Article Online
View Journal

Cite this: DOI: 10.1039/d5tc03093e

Antipolar and short- and long-range magnetic ordering in quasi-two-dimensional $AgCrP_2S_6$

Chaitanya B. Auti, *[a] Atul G. Chakkar, [a] Shantanu Semwal, [b] Sebastian Selter, [c] Yuliia Shemerliuk, [c] Bernd Büchner, [cd] Saicharan Aswartham, [c] Koushik Pal [b] and Pradeep Kumar *[a]

Received 15th August 2025,
Accepted 22nd December 2025

DOI: 10.1039/d5tc03093e

rsc.li/materials-c

$AgCrP_2S_6$ serves as a versatile system to probe dynamics of the quasiparticle excitations as well as multiple phase transitions with lowering temperature linked with the polar, lattice and spin degrees of freedom. Here, we report in-depth temperature- and polarization-dependent Raman scattering measurements on single crystals of quasi-2D zigzag antiferromagnetic $AgCrP_2S_6$, along with first principles-based phonon calculations. We observed multiple phase transitions triggered by the short- and long-range ordering of spins at ~90 K and 20 K, respectively, within the Cr sublattice, where spins are arranged in a 1D chain, as evident from the distinct anomalies in the phonon-mode self-energy parameters and intensity. Contrary to the conventional belief, we proposed the possibility of quasi-antipolar ordering at ~200 K and with further lowering in temperature an antipolar ordering at ~140 K attributed to the Ag ions, which is conjectured to be forbidden owing to the heaviness of Ag ions. The quasi-antipolar and antipolar orderings are gauged *via* a distinct renormalization of the parameters of phonons, which exist at all the temperatures. Additionally, a large number of modes appeared with the decrease in temperature, in the range of ~200–140 K, where antipolar ordering started settling in. The emergence of a large number of phonon modes below ~200 K, nearly double that at room temperature, suggests the lowering of symmetry from high-temperature C_{2h} to low-temperature C_2 or C_s.

1. Introduction

Two-dimensional (2D) van der Waals (vdW) materials have attracted significant attention due to their distinct properties that are advantageous for potential applications in next-generation electronics and advanced physics.[1,2] A significant domain of modern research focuses on magnetic vdW materials that exhibit intriguing physical properties. The intrinsic 2D nature of these materials provides unique opportunities to explore novel magnetic ground states, magnetic excitations, and their interactions with other quasiparticle excitations.[3–6] These tunable properties are of great interest not only for fundamental studies but also for potential applications in advanced fields such as spintronics, optoelectronics, and nanoelectronics.[7,8]

Recently, 2D metal thiophosphates (MTPs) have drawn significant interest because of their intriguing characteristics including magnetism down to monolayer, ferroelectricity, and multiferroicity. The MPS_3 (M = Mn, Fe, Ni, Co, and V) family of layered materials presents a rich array of isostructural compounds that form 2D vdW antiferromagnets.[6,9,10] 2D MPS_3 materials exhibit a wide range of band gaps (~0.24–3.5 eV), which make them highly promising for applications in catalysis, spintronics, and energy conversion.[11] Colombet *et al.* reported that heterocharge substitution also yields numerous stable compounds, which provide an extra degree of freedom in the atomic arrangement.[12,13] One such member of this family is $AgCrP_2S_6$, which exhibits an antiferromagnetic transition temperature (T_N) at ~20 K.[14] The non-magnetic Ag atom and the magnetic Cr atom are arranged in zigzag strips. The Ag^+ ion is bigger in size than the Cr^{3+} ion; as a result, the layer above the Ag atoms significantly bends outward (see SI Fig. S1-(a)[15]). Consequently, a deformation occurs in the P_2S_6 octahedra to accommodate the cations of different sizes. Therefore, to reduce this strain energy, the cations organize themselves in a zigzag chain, and this arrangement functions as a one-dimensional chain of magnetic atoms with a spin value of $S = 3/2$ (see SI Fig. S1-(d)[15]). The layers are arranged in an AAA stacking, resulting in a quasi-2D structure.[16,17]

[a] School of Physical Sciences, Indian Institute of Technology, Mandi-175005, India. E-mail: autichaitanya5@gmail.com, pkumar@iitmandi.ac.in
[b] Department of Physics, Indian Institute of Technology Kanpur, Kanpur 208016, India
[c] Institute for Solid State Research, Leibniz IFW Dresden, Helmholtzstr. 20, 01069 Dresden, Germany
[d] Institute of Solid State and Materials Physics and Würzburg-Dresden Cluster of Excellence ct.qmat, Technische Universität Dresden, 01062 Dresden, Germany

Magnetic fluctuations in 2D structures are influenced by the symmetry of order parameters, namely, the Ising, *XY*, and Heisenberg types.[9] One-dimensional (1D) spin $S = 3/2$ Heisenberg antiferromagnetic Hamiltonian is given as follows:[18]

$$H = -J\sum_i \left(S_i^x S_{i+1}^x + S_i^y S_{i+1}^y + \lambda S_i^z S_{i+1}^z\right) + J'\sum_{i,k} S_i S_k + D\sum_i \left(S_i^z\right),$$

where λ and D denote the exchange and single-ion anisotropy parameters, and S_i^x, S_i^y and S_i^z are the x, y, and z components of the total spin at i^{th} site. J and J' are the intra- and inter-chain exchange coupling constants, respectively. A very small value of $|J'/J| \sim 10^{-4}$ (for $AgCrP_2S_6$) confirm that the system comprises 1D spin chains. The Cr–(P or S)–Cr angle of around 90° allows a strong direct overlap of the octahedrally surrounded Cr's half-filled t_{2g} orbitals.[18] A recent work by Park *et al.*[19] has also suggested that the weakest interaction is interchain, leading to an essentially 1D magnetic behaviour in each layer, while two layers exhibit a weak ferromagnetic coupling. The anisotropic structure introduces an additional degree of freedom, offering the potential to manipulate the material's structure in different ways to provide tunability for probing fundamental magnetism with reduced dimensionality.

Raman spectroscopy is a promising technique for studying the presence of magnons, phase transitions, and various quasiparticle excitations, including spin–phonon and electron–phonon coupling, in 2D magnetic materials.[20–24] Recently, heterocharge MTPs moved into focus due to their low-dimensional magnetism, multiferroicity, and Haldane phase.[25,26] Understanding these singular behaviour in MTPs will provide valuable insights for potential applications in spin-based logic gate devices and non-volatile memory storage devices, opening up the possibility of fabricating heterostructures for multifunctional device applications.[27,28] Motivated by the rich underlying physics in these low-dimensional systems, we conducted an in-depth investigation of the $AgCrP_2S_6$ single crystal using Raman scattering measurements as well as first-principles calculations of the phonons. The current literature lacks information on the temperature-dependent characteristics of phonon and magnetic dynamics, suggesting a potential for uncovering novel insights into the vibrational and magnetic properties of materials.

In this work, we elucidated the phonon excitations and crystal symmetry of $AgCrP_2S_6$ using comprehensive temperature- and polarization-dependent Raman spectroscopy measurements along with the first-principles calculations of phonons. We observed significant hardening of the low-energy phonon modes, attributed to the strong phonon–phonon anharmonic interactions, or an increase in bonding stiffness, indicating structural instability in the material. Based on the temperature-dependent phonon-mode analysis, we observed a signature of antiferromagnetic transition at $T_N \sim 20$ K. Interestingly, we observed anomalies in mode frequency, linewidth, and intensity around temperatures ~90 K, ~140 K, and ~200 K. These transitions are attributed to the possible short-range ordering of the spins and polar ordering in the system, respectively. We also examined the interactions between quasiparticle excitations and electronic and/or magnetic continuums, *i.e.*, Fano asymmetry in the phonon line shape, as a function of temperature. Polarization-dependent measurements show the two-fold symmetry of all the observed modes in line with the group theoretical predictions. Quite surprisingly, we also observed a systematic rotation of the polarization major axis of the phonon modes as a function of temperature. This opens up the possibility of tuning the scattered light in this quasi 2D magnet *via* symmetry control.

2. Experimental and computational details

2.1. Experimental details

The single-crystal samples of $AgCrP_2S_6$ were prepared using a chemical vapor transport technique, as described in ref. 29. Temperature-dependent Raman scattering and photoluminescence (PL) measurements (see the SI for PL measurements[15]) were carried out from 6 to 300 K with ±0.1 K precision with a closed-cycle refrigerator (Montana) and a Horiba LabRAM HR-evolution Raman spectrometer in the backscattering configuration. A 633 nm laser was used to excite the Raman spectra. The laser power was kept very low (<0.5 mW) to prevent local heating. A 50× (NA = 0.5) long-working-distance objective was used to focus the incident laser light on the sample. Scattered light was collected using a Peltier-cooled charge-coupled detector. To unveil the symmetry of phonon modes, polarization-dependent measurements were performed at temperatures of 6 K, 60 K, 120 K, and 170 K. A half-wave plate was placed near the laser entrance to manually rotate the incident polarization onto the sample, while the scattered polarization analyzer remained fixed.

2.2. Computational details

We performed first-principles density functional theory (DFT) calculations using the Vienna *ab initio* simulation package[30,31] and utilized pseudo potentials generated using the projected augmented wave (PAW)[32] method. The valence electron configurations used are $4p^6 4d^{10} 5s^1$, $3d^5 4s^1$, $3s^2 3p^3$, and $3s^2 3p^4$ for Ag, Cr, P and S, respectively. We used Gaussian smearing for treating the partial occupancies for each orbital with an energy broadening of 0.05 eV and treated the exchange–correlation energies of the electrons within the GGA-Perdew–Burke–Ernzerhof (PBE) functional.[33] The cutoff for the kinetic energy was set to 450 eV for all calculations. The primitive cell structure of $AgCrP_2S_6$ contained 20 atoms (2 Ag, 2 Cr, 4 P and 12 S atoms); we considered the antiferromagnetic (AFM) arrangement of Cr atoms and used the DFT-D3 method of Grimme[34] to include the vdW interactions in the structure. The lattice parameters were fully optimized using a k-point grid of $9 \times 9 \times 9$, and the energy convergence criterion was set to 10^{-8} eV. After full optimization, the energies are converged and the force on each atom is of the order of 10^{-4} eV A^{-1} or less. The lattice parameters and volume for the optimized structure were

a = 5.888 A, b = 10.647 A, c = 6.704 A and 403.848 A^3, respectively. The changes in a, b, c and volume are 0.09%, 0.24%, −0.6% and 0.3%, respectively, when compared with the experimental lattice parameters.

The phonon calculations were performed using the finite-difference method as implemented in Phonopy.[35,36] We used a 2 × 2 × 2 supercell containing 160 atoms, considering the AFM arrangement of Cr atoms and including the vdW interactions. The tabulated frequencies and symmetry labels of all the modes at Γ-point are provided in Table S2.

3. Results and discussion

3.1 Crystal structure and phonon modes

$AgCrP_2S_6$ exhibits a monoclinic symmetry having the space group $P2/a$ (#13) and the point group C_{2h} ($2/m$). The unit cell of the $AgCrP_2S_6$ bulk single crystal consists of 60 phonon modes at the Γ-point of the Brillouin zone, with the following irreducible representations:[37] $\Gamma_{total} = 14A_g + 14A_u + 16B_g + 16B_u$. There are 30 Raman active ($\Gamma_{Raman} = 14A_g + 16B_g$) modes and 27 infrared active ($\Gamma_{IR} = 13A_u + 14B_u$) modes (for more details, see Table 1). The Raman spectra is recorded using 633 nm laser excitation, and 48/27 Raman modes are observed at 6 K/300 K, which are labelled as P1–P48 at 6 K, as shown in Fig. S2. To extract the self-energy parameters of phonon modes, *i.e.*, peak frequency (ω), full width at half maximum (FWHM), and intensity, spectra are fitted using a sum of Lorentzian functions. We also recorded the spectra in the higher frequency range of 700–1400 cm^{-1} and observed some very weak higher order modes, as shown in SI Fig. S9.[15] Fig. 1(a) and (b) show the temperature evolution of the Raman spectrum of $AgCrP_2S_6$ in the temperature range of 6 to 300 K from 15 to 350 cm^{-1} and 350 to 700 cm^{-1} (magnified spectra in the smaller spectral range are shown in SI Fig. S6–S8[15]).

All higher frequency modes ranging from ∼250 cm^{-1} soften with the increase in temperature, showing a normal anharmonic phonon behaviour; while some lower frequency range modes show anomalous hardening, and others show a softening and get broadened with the increase in temperature. In the $M_2P_2S_6$ material family, the higher frequency (above ∼250 cm^{-1}) modes are assigned to the vibration due to P_2S_6 octahedra; therefore, these modes are similar in all $M_2P_2S_6$ compounds, and the lower frequency (below ∼250 cm^{-1}) Raman modes are assigned to the heavy metal ion.[38] The particular M atom determines the cutoff frequency that separates the high- and low-frequency regimes. Phonon dispersion along with the atom-resolved phonon density of state (phdos) is shown in Fig. 2a and b, respectively. From the atom-resolved phdos shown in Fig. 2b, we can see that in the high-frequency region (500 cm^{-1} to 650 cm^{-1}), the contributions to the phonon dispersion are mainly due to the P and S atoms due to smaller masses of these atoms. In the middle region (150 cm^{-1} to 500 cm^{-1}), we see the P contribution waning and being taken over by the S atoms and rising contribution due to Cr seen around 350 cm^{-1}, 300 cm^{-1}, and 200 cm^{-1}. Finally, in the lower frequency region (20 cm^{-1} to 150 cm^{-1}), we see the contributions of S, P and Cr decreasing and the Ag contributions increasing with large Ag localization having peaks around 60 cm^{-1} and 20 cm^{-1} to 40 cm^{-1}. All prominent phonon-mode intensities reduce drastically from the lowest recorded temperature to the highest temperature, as shown in Fig. 1(a) and (b). The most intense phonon mode P19 could be a mode associated with the anionic complex $[P_2S_6]^{4-}$, which is almost twice as intense as the other prominent modes P11, P33, and P47. Many phonon modes as P4, P5, P9, P15, P16, P17, P20, P23, P25, P29, P31, P32, P34, P35, P36, P40, P41, P42, P44, and P48 disappear with the increase in temperature (see Fig. S3, which shows disappeared phonon modes). Mode P31 (∼469.5 cm^{-1} at 6 K) shows an asymmetric line shape (see Fig. 4(c)), as discussed in detail in Section 3.4.

Table 1 Wyckoff positions of atoms and irreducible representations of the phonon modes for $AgCrP_2S_6$ in the monoclinic ($P2/a$; #13) crystal system

Atoms	Wyckoff position	Mode decomposition	Raman tensors
Ag	2e	$A_g + A_u + 2B_g + 2B_u$	$A_g = \begin{pmatrix} b & 0 & d \\ 0 & c & 0 \\ d & 0 & a \end{pmatrix}$
Cr	2e	$A_g + A_u + 2B_g + 2B_u$	
P	4g	$3A_g + 3A_u + 3B_g + 3B_u$	
S	4g	$3A_g + 3A_u + 3B_g + 3B_u$	$B_g = \begin{pmatrix} 0 & f & 0 \\ f & 0 & e \\ 0 & e & 0 \end{pmatrix}$
S	4g	$3A_g + 3A_u + 3B_g + 3B_u$	
S	4g	$3A_g + 3A_u + 3B_g + 3B_u$	

$\Gamma_{total} = 14A_g + 14A_u + 16B_g + 16B_u$;
$\Gamma_{Raman} = 14A_g + 16B_g$; $\Gamma_{IR} = 13A_u + 14B_u$; $\Gamma_{Acoustic} = A_u + 2B_u$

3.2 Temperature dependence of the phonon modes

Generally, mode frequencies are expected to exhibit softening with the increase in temperature.[39] Fig. 3 shows the temperature dependence of frequency and the FWHM of some of the prominent phonon modes labelled as P2, P3, P5, P7, P8, and P10–P14 (for more phonon modes, see SI Fig. S4[15]). Some intriguing features are observed: (i) for the lower frequency range $\omega \leq 250$ cm^{-1}, some of the phonon modes P2, P3, P7, P10, P12, and P14 show abnormal hardening with the increase in temperature. (ii) A rapid decrease in the intensity of the phonon modes P10 and P14 with the increase in temperature (see Fig. 4(a)). (iii) Many phonon modes disappear with the increase in temperature (see SI Fig. S3[15]). Interestingly, the mode P7 shows abnormal hardening with the increase in temperature and approaches towards P8 (ω_{P8} = 159.5 cm^{-1} at room temperature). The mode P10 approaches P11 with a sharp increase in frequency $\Delta\omega_{P10} \sim 12$ cm^{-1}. However, P13 and P14 diverge from each other with the increase in temperature (see Fig. 4(b)). P2 and P3 both show abnormal hardening with the increase in temperature. These modes may be associated with the heavy metal ion Ag^+.[16] The possible reasons associated with the anomalous frequency change are discussed in detail in Section 3.3.

3.2.1 Anomalous temperature dependence of the phonon modes. Interestingly, phonon modes P5, P6, P8, P12, P13, P14, P19, P21, and P47 exhibit anomalous softening in frequency

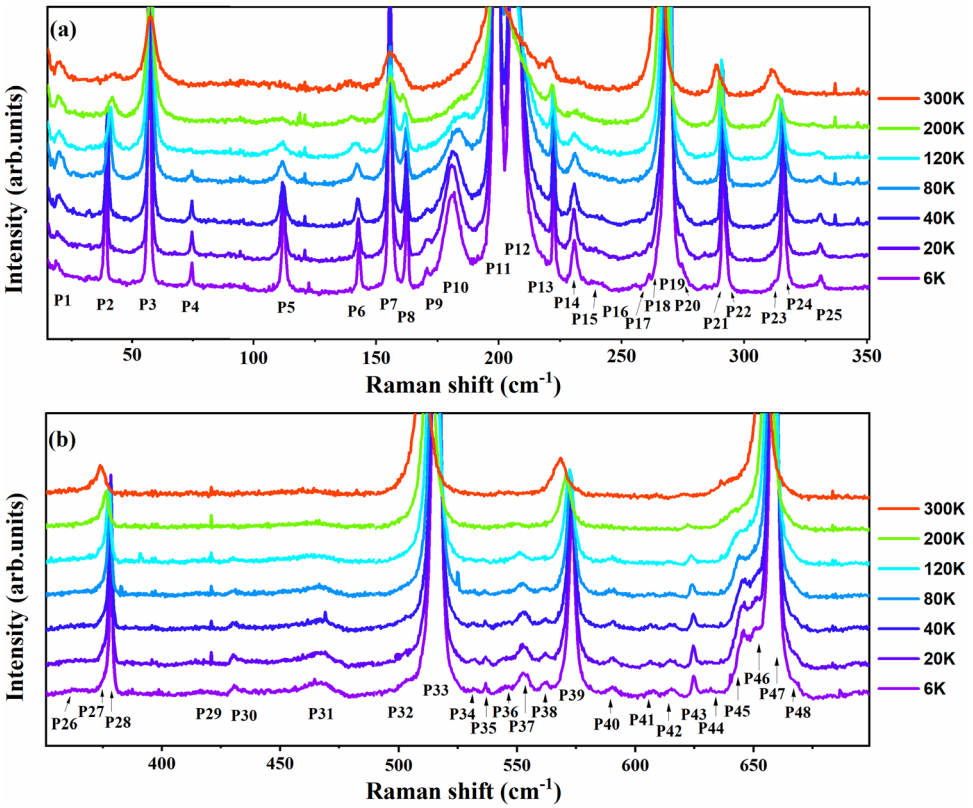

Fig. 1 Temperature evolution of the Raman spectrum in the temperature range of 6 to 300 K, ranging from (a) 15–350 cm^{-1} and (b) 350–700 cm^{-1}. The observed phonon modes are labelled as P1–P48.

below temperature ~20 K, *i.e.*, antiferromagnetic ordering T_N (~20 K). The FWHM of the modes P2, P3, P7, P8, P10, and P13 also shows a change in slope at ~T_N. This anomalous nature of the phonon modes below T_N may be attributed to the spin–phonon coupling. It is noted that spin–phonon coupling is generally expected to be effective only up to a long-range ordering temperature where the long-range magnetic correlations exist.[40–42]

We note that at room temperature, several phonon modes are relatively broad (see Fig. 1(a), (b) and Fig. S6–S8[15]), evolving into much sharper modes at low temperatures. While such behaviour is consistent with anharmonic phonon–phonon interactions, the relatively large linewidth changes observed for low-frequency modes such as P2, P3, P7, P11, and P12 of ~75% ($|(\omega_{6K} - \omega_{300K})|/\omega_{300K}$) (see Fig. 3) may also suggest a possible contribution from additional temperature-dependent lattice fluctuations and the presence of Ag^+ cation disorders at high temperatures.

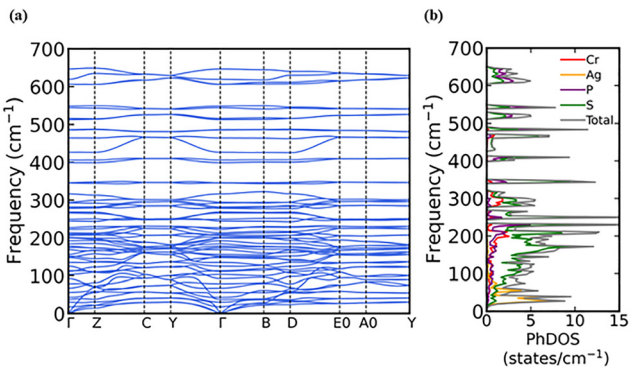

Fig. 2 (a) Phonon dispersion and (b) atom-resolved phonon density of states based on the AFM arrangement of $AgCrP_2S_6$ and including the vdW forces.

It is noteworthy that several phonon modes P5, P6, P8, P13, P19, P21, P24, P28, P33, P39, and P47 show a change in the slope of their frequency shifts ~90 K (see Fig. 3 and Fig. S4[15]). The mode P3 exhibits a sharp frequency increase up to ~90 K, remaining nearly constant thereafter. The FWHM of modes P13, P28, P45, and P47 also shows slope changes at ~90 K, indicating a clear anomaly. In addition, the mode P10 shows a slight kink at ~140 K, while the modes P13, P19, and P21 display discontinuities in frequency at this temperature. The FWHM of phonon modes P6, P10, and P14 exhibits a jump at ~140 K, while modes P8, P19, and P47 show a change in slope, indicating an anomaly at this temperature. Around 200 K, mode P2 displays a discontinuity in frequency, and modes P8, P19, P21, and P39 show slope changes in their frequency shifts. Mode P12 exhibits an unusual hardening behaviour above 200 K, with its frequency increasing from ~204.5 to ~209 cm^{-1} with the increase in temperature from 200 K to ~300 K, marking a clear anomaly near 200 K. Additionally, the FWHM of modes P6 and P10 shows a jump, and that of modes

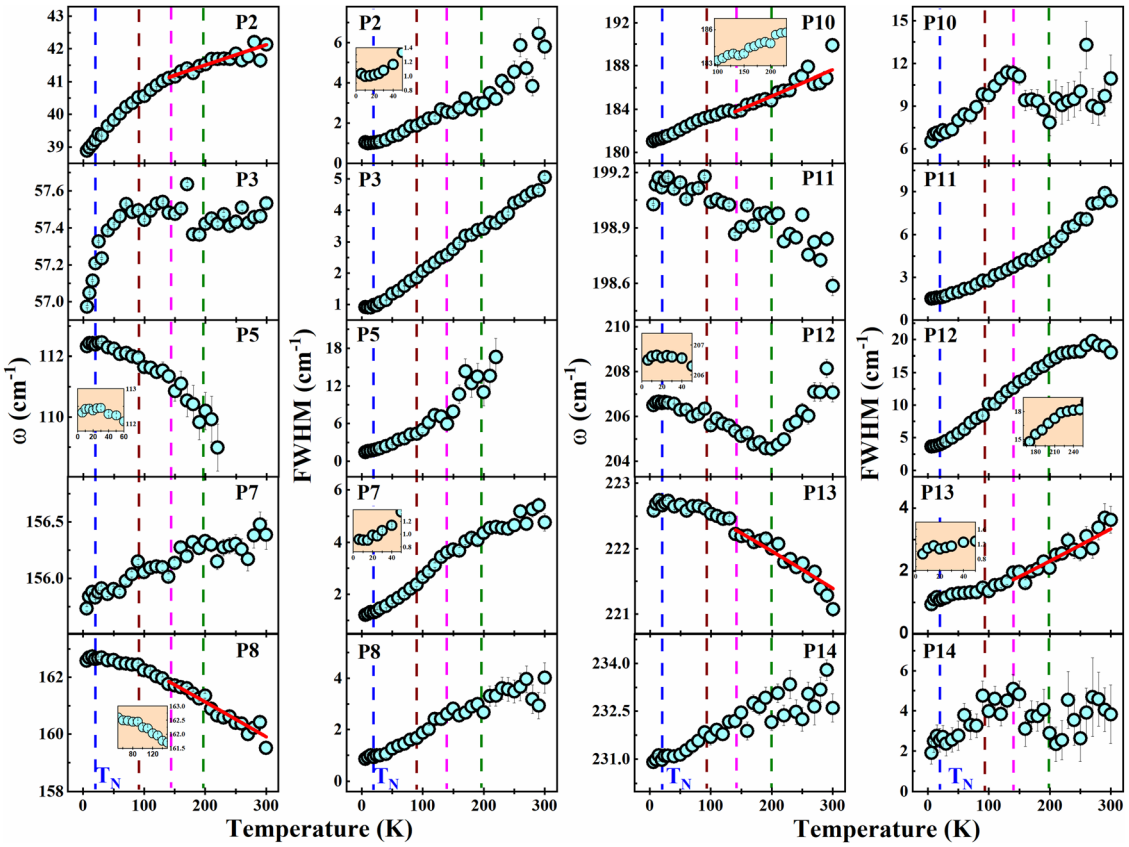

Fig. 3 Temperature evolution of the mode frequency and FWHM of phonon modes P2, P3, P5, P7, P8, and P10–P14. The solid red line shows a three-phonon fitting in the temperature range 140 K to 300 K. The dashed blue line indicates the antiferromagnetic transition at ∼20 K, while the dashed brown, pink, and green lines indicate anomalies around ∼90 K, ∼140 K, and ∼200 K, respectively. The insets show magnified views of the corresponding anomalies in both frequency and FWHM.

P7, P12, P19, and P21 shows slope changes around this temperature; the lifetime of the phonons is strongly influenced in the vicinity of this temperature. Moreover, many phonon modes start appearing below ∼200 K and continue to emerge till ∼140 K (see SI Fig. S3[15]), consistent with the anomalies observed in the modes which survive at all the temperatures.

Interestingly, the intensity change of all the phonon modes with temperature is nearly uniform except for the modes P10 and P14, whose intensity decreases sharply with the increase in temperature by ∼10 times compared to its intensity at 6 K, as shown in Fig. 4(a). Phonon modes P2 and P3 show very interesting intensity variation; their intensity increases with the increase in temperature up to ∼90 K, after which it decreases, indicating an anomaly at ∼90 K. We note that a similar intensity behaviour is also reported for the low-frequency modes in a sister compound, *i.e.* $CuCrP_2S_6$, which suggests that the lattice dynamics of off-centre Cu^+ cations within the intralayer is not quenched, indicating that an order–disorder type of structural transition is responsible for the emergence of defect dipoles associated with Cu ions.[43] It is observed that the intensity of the modes P7, P10, P11, P13, P14 and P19 shows a sharp decrease with the increase in temperature and remains nearly constant after 200 K, clearly showing an anomaly at ∼200 K (see Fig. 4(a) and Fig. S5[15]).

3.2.2 Discussion for phonon anomalies. The origin of the anomalies in phonon frequency, linewidth, and intensity at ∼90 K, 140 K, and 200 K is not exactly pinpointed. The anomaly at ∼90 K is suggestive of the development of short-range magnetic correlations. Previous magnetic susceptibility data show a broad maximum in the susceptibility well above T_N, which is typically associated with the short-range ordering.[19] A related system, $AgCrP_2Se_6$, reports that a substantial fraction of the entropy is released above the Néel temperature, suggesting that short-range ferromagnetic ordering exists above T_N, again hinting that short-range correlations could be possible in these types of systems.[44] Moreover, the exchange parameter for $AgCrP_2S_6$ was estimated to be of the order of $J \sim 9$ meV (∼100 K);[14] therefore, the observed changes in the phonon modes around 90 K may be associated with the short-range ordering. We note that its sister compound, *i.e.* $CuCrP_2S_6$, undergoes antiferroelectric and antiferromagnetic ordering attributed to the Cu^+ and Cr^{3+} cations, respectively. It undergoes a phase transition from a room-temperature paraelectric state (space group $C2/c$ and point group C_{2h}) to a quasi-antipolar state at ∼190 K (space group P_c and point group C_s). In addition, with the further lowering of temperature, it goes to a fully antiferroelectric phase at ∼145 K with the space group P_c. This has been attributed to the ordering of Cu ions

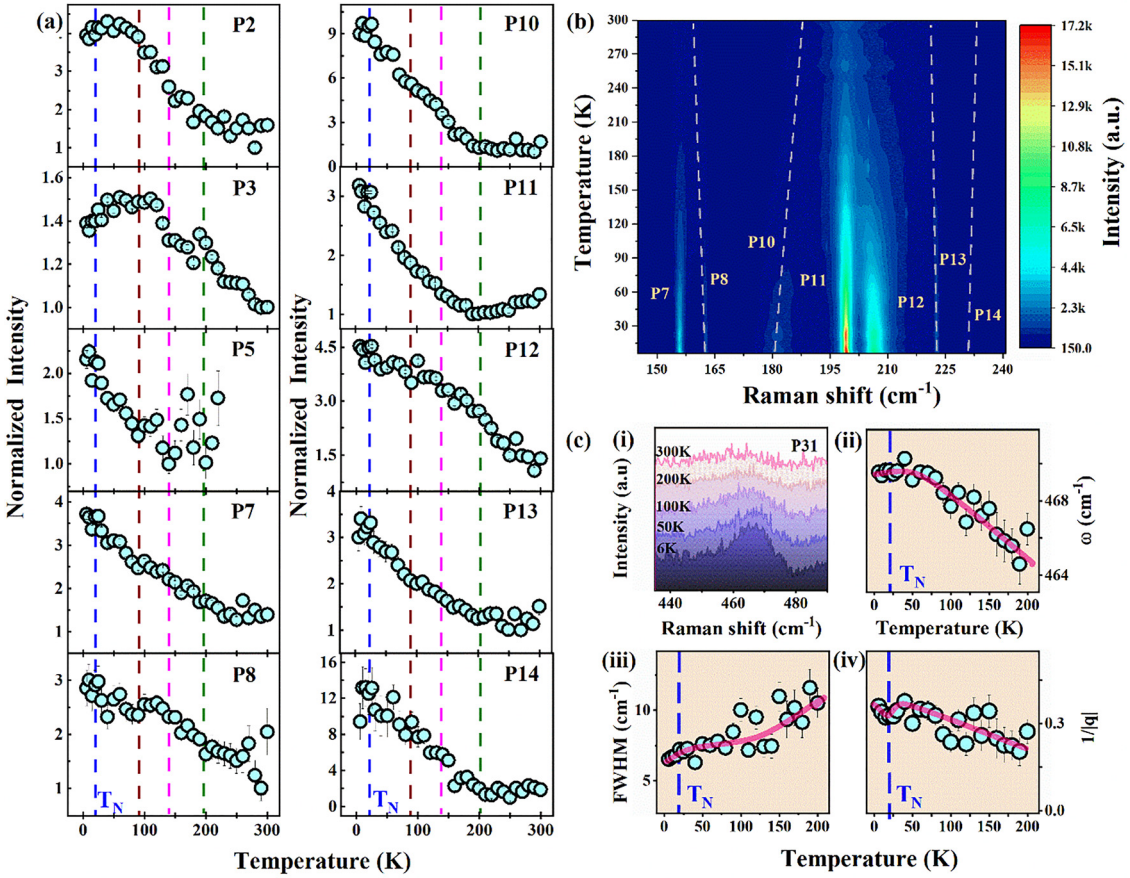

Fig. 4 (a) Temperature dependence of the normalised intensity of modes P2, P3, P5, P7, P8, and P10–P14. (b) Colour contour plot of the phonon intensity in the temperature-Raman-shift plane. The vertical dashed line marks the corresponding mode evolution. (c) (i) Temperature evolution of the Fano mode P31. (ii)–(iv) Temperature dependence of frequency, FWHM and the coupling strength (1/|q|) of mode P31 in the temperature range of 6 K to 200 K. The solid semi-transparent pink line is drawn as a guide to the eye.

within the lamellae. Additionally, across the antipolar phase transition at ∼145 K, it shows negative thermal expansion.[21] However, for $AgCrP_2S_6$, it is advocated that since Ag^+ is a heavier cation, it will not dislocate in the lattice, and hence, no ferroelectric transition is expected.[45] It is also possible that subtle local distortions associated with antipolar and quasi-antipolar orders may exist, which could be reflected in localized probes such as Raman spectroscopy. Moreover, for $AgCrP_2Se_6$, two higher temperature transitions have been reported at ∼68 K and 125 K, other than the low-temperature antiferromagnetic transition at ∼42 K.[44] The two transitions are attributed to the possible ferroelectric/antiferroelectric ordering due to lattice restructuring involving Ag ions. Moreover, a negative thermal expansion is reported around 180 K. We note that Cu ion hopping is responsible for the ionic conductivity in $CuCrP_2S_6$. Ionic conductivity in $AgCrP_2S_6$ is low compared to $CuCrP_2S_6$, as also reflected from their activation energy (1.26/0.67 eV for (Ag/Cu)CrPS).[45] The hopping of Ag ions in $AgCrP_2S_6$ cannot be ruled out, though the hopping may be limited, and hence, there is a possibility of an antipolar ordering similar to $CuCrP_2S_6$. Our observations of soft phonon-like modes (discussed in detailed in Section 3.3) and observed anomalies in the phonon modes suggest that, despite the heaviness of the Ag^+ ion, the antipolar and quasi-antipolar phase transitions cannot be ruled out in $AgCrP_2S_6$. Our observations suggest several contributing factors for this anomalous trend of the phonon modes, as discussed in Section 3.3. One possible explanation is that local structural contraction may be associated with the Ag^+ and Cr^{3+} cation structures. Nevertheless, our observations of distinct changes in the mode frequency, linewidth, and intensity suggest the possibility of multiple phase transitions in $AgCrP_2S_6$. Thus far, no transport measurements have been done on this material to confirm a ferroelectric transition. This is an important open question. Our observation calls for further theoretical and experimental studies to shed more light on the complex physics associated with this system, particularly the ambiguity surrounding the polar/anti-polar ordering and related phonon anharmonicities.

3.2.3 Emergence of new phonon modes at low temperatures. Irreducible phonon mode calculations show that there are only 30 Raman active modes, but we have observed a total of 48 phonon modes at the lowest temperature, including some weak modes (see Table S1[15]). As the temperature increases, several modes disappear, with the total number reducing to

nearly half, *i.e.* 27, of that observed at low temperatures, as shown in Fig. S3. While decreasing the temperature, we notice that many new modes start appearing in the temperature window of ~140–200 K, as expected for a first-order character of the antiferroelectric transition. We note that with the increase in temperature from 6 K, modes involving dynamics of metal ions soften and broaden and, finally, disappear around 140–200 K. For example, the low-frequency mode P4/P5, see Fig. 3 and Fig. S4, softens by ~2.5/3% and disappears at ~140/200 K. The disappearance of these phonon modes along with many other modes with the increase in temperature can be attributed to several factors including thermal broadening, increased anharmonic phonon–phonon interactions, and reduced phonon lifetime, which result in an increase in FWHM. Additionally, structural instability in the symmetry may contribute to the suppression of certain modes at elevated temperatures.[46] As outlined in the review by S. Kamba,[47] displacive ferroelectric transitions are typically characterized by the softening of optical phonon modes, where the frequency of the soft mode continuously decreases and ideally approaches zero at the critical temperature (T_C), indicating a lattice instability. In contrast, order–disorder transitions are governed by the relaxational dynamics of ions or dipoles hopping between equilibrium positions, and the characteristic frequency slowing is generally observed in the microwave to a low-frequency regime rather than in the optical phonon spectrum. Here, we observed low-frequency soft phonon-like modes (P2, P3, P7, P10, P12, and P14) whose frequency decreases with the decrease in temperature but does not approach zero at T_C, indicating the absence of a purely displacive mechanism. Observed phonon anomalies in phonon self-energy parameters, along with the emergence of new modes, suggest a more complex behaviour possibly involving structural transition and ordering of Ag ions within the lattice. This scenario points towards an order–disorder-type transition with contributions from coupled lattice instabilities. A similar ambiguity exists in the case of $CuCrP_2S_6$, where an order–disorder transition is suggested,[43] yet soft-mode-like features have been reported.[48] Therefore, it is likely that similar to its sister compound $CuCrP_2S_6$, $AgCrP_2S_6$ also undergoes order–disorder type of structural transition and is also responsible for the potential polar ordering.

Our observations clearly favour the possibility of structural instability, with singular changes in self-energy parameters of the prominent modes, which survive at all the temperatures. We note that the symmetry of the newly emerged modes at low temperatures (see Fig. S12 and S13[15]) is also similar to the modes at high temperatures. This reflects that the symmetry of the modes is the same, but their number becomes nearly double, *i.e.* going to the lower symmetry (C_2 or C_s) as the temperature is decreased. Our observation of emergence of new modes in the temperature interval of ~140–200 K and modes showing distinct anomalies at these temperatures suggest a symmetry-lowering structural transition from a high-temperature C_{2h} point group to C_2 or C_s point groups at these temperatures.[21]

3.3 Discussion on anomalous hardening of the phonon modes

Anomalous hardening of the low-frequency phonon modes P2, P3, P7, P10, P12 and P14 may be associated with the anharmonic effects, which comes into the picture due to (i) strong phonon–phonon anharmonic interactions and (ii) lattice thermal contraction or structural instability, which are discussed as follows:

3.3.1 Strong phonon–phonon anharmonic interactions. Generally, with the increase in temperature, a phonon mode softens. However, strong phonon–phonon anharmonic interactions may lead to phonon hardening with the increase in temperature,[49] and this abnormal phonon hardening in our case may also favour a possible transition based on the large atomic displacement, *i.e.* antiferroelectric transition. These interactions play a crucial role in determining the ground state of incipient ferroelectrics. The self-energy of a phonon is given as $\Sigma = \Sigma_r + i\Sigma_i$, imaginary part ($\Sigma_i$) is related to the lifetime of a phonon, and for a given phonon, it is a function of ω and T given as $\Delta\Gamma(T) \propto \Sigma_i(\omega) \propto |V|^2\rho_2(\omega, T)$, where V is the average anharmonic coupling constant and $\rho_2(\omega)$ is the two-phonon density of states with the restrictions of momentum conservation and $\omega = \omega_1 + \omega_2$. The real part, Σ_r, is associated with the phonon frequency given as follows:

$$\Delta\omega(T) \propto \Sigma_r = \frac{2|V|^2}{\pi}\int_0^\infty \frac{\rho_2(\omega', T)}{\omega^2(T) - \omega'^2}\mathrm{d}\omega', \quad (1)$$

for simplicity, V is assumed as independent of frequency. The sign of this integral determines the sign of the self-energy constant (A), which is generally negative due to the dominance of the term with $\omega' > \omega$. Conversely, if the peak in the two-phonon density of states is lower than ω, the integral may give a positive value, potentially resulting in a hardening of the phonon modes.[49,50] Our observation of the anomalous hardening of the mode P2, P3, P7, P10, P12, and P14 clearly reflects strong phonon–phonon anharmonic interaction, suggesting a large movement of ions. We note that these low-frequency modes are associated with the motion of heavy ions Ag^+/Cr^{3+}, and these ions are the ones where displacement is potentially responsible for the antiferroelectric transition in this class of material. Therefore, based on the anomalies observed here, we also suggest that these anomalies in this system are potentially related to the potential antipolar ordering.

Now to understand the impact of anharmonicity on the frequency and FWHM of the phonon modes in the temperature range of ~140 to 300 K, we used an anharmonic three-phonon model, given as follows:[39,51]

$$\Delta\omega = \omega(T) - \omega_0 = A\left(1 + \frac{2}{e^x - 1}\right), \quad (2)$$

$$\Delta\Gamma = \Gamma(T) - \Gamma_0 = C\left(1 + \frac{2}{e^x - 1}\right), \quad (3)$$

where ω_0 and Γ_0 represent the mode frequency and FWHM at absolute zero temperature, respectively, and $x = \frac{\hbar\omega_0}{2k_BT}$. A and C

represent the self-energy constant that describes the strength of phonon–phonon interactions involving three phonon processes. Anharmonic model fit to the experimental data for the case of frequency and FWHM is shown by solid red lines in the temperature range of 140–300 K. Fig. 3 illustrates the prominent modes fitted (frequency and FWHM) using eqn (2) and (3), respectively. The optimal parameters are shown in Table S3. The self-energy constant (A) associated with the modes P2 and P10 is positive, indicating that the term $\omega > \omega'$ is dominant in eqn (1) for these modes, while for all other phonon modes, it is negative.

3.3.2 Lattice thermal contraction or structural instability. Temperature-dependent behaviour of the phonon modes is closely related to the direction (symmetry) and magnitude of lattice vibrations; anomalous phonon mode behaviour may arise from their anisotropic structural properties. Hardening of the low-frequency phonon modes with the increase in temperature indicates that bonding stiffness corresponding to these modes increases, suggesting that there may be a local structural instability.[52] This type of behaviour of phonon modes is referred to as soft phonon modes, *i.e.*, their frequency decreases with the decrease in temperature. The soft mode-like behaviour is understood within the mean field approximation[43,53] $\omega(T) = \beta(T^* - T)^{1/2} + \omega_0$, where β is a constant and T^* is the characteristic temperature at which a mode disappears. As clear from our observation T^* is found to be in the range of ~140–200 K. We note that the frequency of these modes does not go to zero across T^*, unlike the soft phonon mode expected in a displacive-type structural transition. The presence of the second term ω_0 favours the view point that the quasi-antipolar order is also present in this system similar to the compound $CuCrP_2S_6$ and is driven by an order–disorder transition rather than the condensation of a soft phonon mode. Many of the low-frequency phonon modes (P2, P3, P7, P10, P12, and P14; see Fig. 3) associated with the motion of metal cations show anomalous softening. This anomalous behaviour may be associated with the interlayer silver ion hopping. We note that a similar behaviour is also reported for a phonon mode in $CuCrP_2S_6$.[43] Therefore, our observations of anomalous softening of the low-frequency modes in $AgCrP_2S_6$ suggest the possibility of quasi-antiferroelectric and subsequently antiferroelectric ordering in the temperature window of ~200–140 K.

3.4 Fano resonance

We observed that the phonon mode P31 exhibits an asymmetric line shape, which can be attributed to the interaction between the discrete phonon and an underlying magnetic or electronic continuum. In $AgCrP_2S_6$, an electronic origin of the continuum can be ruled out, since the optical band gap lies far above the Raman excitation energy (~1.32 eV at 6 K), making the electronic contribution negligible. Therefore, the continuum responsible for the Fano asymmetry is most likely magnetic in nature. This suggests that the asymmetric profile of the P31 mode originates from magnetic fluctuations within the Cr sublattice, indicative of a spin–phonon coupling mechanism. Such asymmetry is well described by the Breit–Wigner–Fano (BWF) function as[54] $I(\omega) = I_0\frac{[1 + (\omega - \omega_0)/q\Gamma]^2}{1 + [(\omega - \omega_0)/\Gamma]^2}$, where ω_0 and Γ are the frequency and FWHM of the uncoupled phonon, respectively. q is the asymmetry parameter that characterizes the coupling strength between the phonon and the continuum, quantified by the parameter $1/|q|$. Microscopically $1/|q| \propto |V_E|$, where $|V_E|$ tells the interaction between the discrete state and the continuum. Therefore, limit $1/|q| \to 0$ corresponds to weak coupling, which causes the peak to be symmetric and reduces to a Lorentzian line shape; and limit $1/|q| \to \infty$ represents strong coupling that causes the peak to be more asymmetric. Fig. 4(c-i) show the temperature evolution of the asymmetric mode P31 in the temperature range of 6–300 K. Fig. 4(c-ii) and (c-iii) show the temperature dependence of the frequency and FWHM of mode P31 in the temperature range of 6–200 K. For mode P31, as the temperature increases, the frequency decreases and the FWHM increases, with a change in slope for both parameters occurring around T_N (~20 K). Fig. 4(c-iv) shows the temperature dependence of the coupling strength ($1/|q|$), and it decreases with the increase in temperature with a jump around T_N (~20 K). This suggests that the coupling between phonon and underlying magnetic continuum is strongly affected by long-range magnetic ordering.

4. Polarization dependence of the phonon modes

To determine the symmetry and to understand the angle-dependent characteristics of the phonon modes, we carried out in-depth polarization-dependent Raman measurements at four temperatures: 6 K, 60 K, 120 K, and 170 K, as shown in Fig. 5, for few selected modes (for more phonon modes, see SI Fig. S10 and S11[15]). The angular dependence of the phonon mode intensity is given by eqn (4) and (5), considering the complex element of the Raman tensor (see Section S1 in the SI for polarization intensity analysis details[15]):

$$I_{A_g} = |b|^2\cos^2(\theta + \theta_0)\cos^2\theta_0 + |c|^2\sin^2(\theta + \theta_0)\sin^2\theta_0 + 2|b||c|\cos(\theta + \theta_0)\cos\theta_0\sin(\theta + \theta_0)\sin\theta_0\cos\phi_{bc} \quad (4)$$

$$I_{B_g} = |f|^2\sin^2(\theta + 2\theta_0), \quad (5)$$

where $\phi_{bc} = \phi_b - \phi_c$ is the phase difference between the b and c components of the Raman tensor.

In Fig. 5 (SI Fig. S10 and S11[15]), the solid red line shows the fitted curves using eqn (4) and (5).

Fig. 5 shows the polar plot for the intensity of the modes P7, P8, P13, P19, and P47 at four different temperatures. The mode P7 shows the quasi-isotropic behaviour at 6 K, and it approaches a two-fold symmetry at 60 K; and it shows a complete two-fold symmetry at higher temperatures of 120 and 170 K with maxima around 20 and 200 degrees. The mode P8 shows the two-fold symmetry at all four temperatures, with maxima around 40 and 220 degrees. The mode P47 shows the quasi-isotropic behaviour at 6 and 60 K, while it becomes

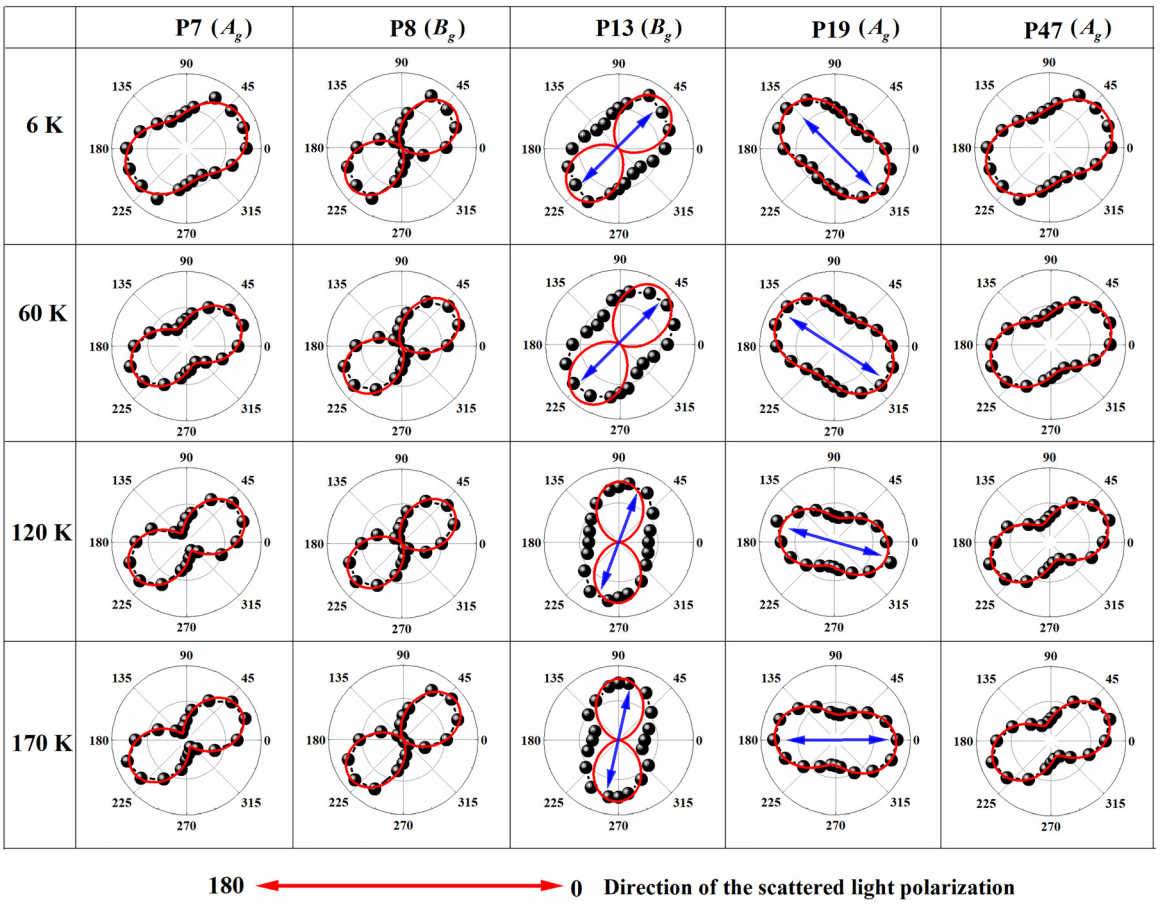

Fig. 5 Polarization-dependent intensity profiles of phonon modes P7, P8, P13, P19, and P47 measured at 6 K, 60 K, 120 K, and 170 K, respectively, under varying incident-light polarization. Blue arrows represent the rotation of the axis, showing the maxima as a function of temperature. The solid red line at the bottom indicates the direction of the scattered light polarization.

two-fold at 120 and 170 K with maxima around 20 and 200 degrees. The modes that disappeared at higher temperatures also exhibit a twofold symmetry, as shown in SI Fig. S12 and S13.[15] This reflects that the symmetry of these modes is also A_g/B_g or A/B consistent with the group theoretical arguments. Interestingly, mode P13 shows the quasi-isotropic behaviour with maxima around 40 and 220 degrees at 6 and 60 K, while at higher temperatures of 120 and 170 K, it shows the maxima around 90 and 270 degrees. Moreover, the modes P19 and P33 (see Fig. S11) show maxima at $\sim$140 and 320 degrees at 6 and 60 K, while at higher temperatures, it shows maxima at $\sim$0 and 180 degrees. Such rotation in the polar plots likely originates from subtle structural changes or distortions that modify the Raman tensor elements at lower temperatures. The magneto-optical Kerr effect can be ruled out as the primary cause, since the observed rotation is not uniform across all phonon modes and occurs well above the magnetic ordering temperature, where long-range magnetic order is absent. The possibility of birefringence-induced rotation is also less probable, as the effect is strongly mode-selective and does not show the uniform angular dependence characteristic of optical birefringence. Instead, a more probable origin could be strain-induced local anisotropy or temperature-driven structural distortion, both of which can locally modify the polarizability tensor and give rise to the observed rotation in certain phonon modes. We note that a similar rotation has also been reported recently in other 2D magnetic systems.[5,55] The microscopic understanding of these rotations and changes in the symmetry from quasi-isotropic behaviour to twofold symmetry as a function of temperature calls for a detailed theoretical study to uncover the mechanisms underlying these changes.

5. Conclusion

In conclusion, we performed comprehensive temperature- and polarization-dependent Raman measurements on single-crystal $AgCrP_2S_6$ along with the first-principles-based calculations of phonons. Our results have shown that this quasi-2D van der Waals material, $AgCrP_2S_6$, with 1D spin chains demonstrated a possibility of quasi-antipolar and antipolar phase transitions in contrast to the conventional view so far adopted in the literature, therefore putting forward that even the heavy ion (Ag)-based system may show antiferroelectric ordering. Our findings also pave the way forward for potentially controlling and manipulating these orderings as a function of layer and making

them useful for potential applications. We also observed the signature of a long-range magnetic ordering at low temperatures, and all these transitions are marked by the distinct renormalization of the phonon modes as well as the emergence of multiple phonon modes with the decrease in temperature. Our findings indicated that this material may also be tuned as a potential multiferroic material similar to its sister compounds. Additionally, polarization-dependent measurements elucidate the role of anisotropy in the system, shedding light on the crystal symmetry. Our findings offer critical insights into the phonon dynamics of this quasi-2D magnetic compound, providing a deeper understanding of its underlying mechanisms.

Author contributions

Chaitanya B. Auti: writing, review and editing, writing – original draft, investigation, data curation, formal analysis, methodology. Atul G. Chakkar: data curation, formal analysis, writing – review & editing. Shantanu Semwal: data curation, formal analysis, writing – review & editing. Sebastian Selter: formal analysis, writing – review & editing. Yuliia Shemerliuk: formal analysis, writing – review & editing. Bernd Büchner: formal analysis, writing – review & editing. Saicharan Aswartham: formal analysis, writing – review & editing. Koushik Pal: data curation, formal analysis, writing – review & editing. Pradeep Kumar: formal analysis, funding acquisition, supervision, validation, methodology, writing – review & editing.

Conflicts of interest

There are no conflicts to declare.

Data availability

All the data that support the findings of this study are included within the article and supplementary information (SI). Supplementary information is available. See DOI: https://doi.org/10.1039/d5tc03093e.

Acknowledgements

P. K. thanks SERB (project no. CRG/2023/002069) for the financial support and IIT Mandi for the experimental facilities.

References

1 C. Liu, H. Chen, S. Wang, Q. Liu, Y.-G. Jiang, D. W. Zhang, M. Liu and P. Zhou, Two-dimensional materials for next-generation computing technologies, *Nat. Nanotechnol.*, 2020, **15**, 545.
2 L. Liao, E. Kovalska, J. Regner, Q. Song and Z. Sofer, Two-Dimensional van der Waals Thin Film and Device, *Small*, 2024, **20**, 2303638.
3 T. T. Mai, K. F. Garrity, A. McCreary, J. Argo, J. R. Simpson, V. Doan-Nguyen, R. V. Aguilar and A. R. H. Walker, Magnon–phonon hybridization in 2D antiferromagnet $MnPSe_3$, *Sci. Adv.*, 2021, **7**, eabj3106.
4 S. Liu, A. Granados del Águila, D. Bhowmick, C. K. Gan, T. Thu Ha Do, M. A. Prosnikov, D. Sedmidubský, Z. Sofer, P. C. M. Christianen and P. Sengupta, Direct observation of magnon–phonon strong coupling in two-dimensional antiferromagnet at high magnetic fields, *Phys. Rev. Lett.*, 2021, **127**, 097401.
5 A. G. Chakkar, D. Kumar and P. Kumar, Broken weak and strong spin rotational symmetries and tunable interactions between phonons and the continuum in $Cr_2Ge_2Te_6$, *Phys. Rev. B*, 2024, **109**, 134406.
6 N. Khan, D. Kumar, V. Kumar, Y. Shemerliuk, S. Selter, B. Büchner, K. Pal, S. Aswartham and P. Kumar, The interplay of topology and antiferromagnetic order in two-dimensional van der Waals crystals of $(Ni_xFe_{1-x})_2P_2S_6$, *2D Mater.*, 2024, **11**, 035018.
7 H. Li, S. Ruan and Y.-J. Zeng, Intrinsic van der Waals Magnetic Materials from Bulk to the 2D Limit: New Frontiers of Spintronics, *Adv. Mater.*, 2019, **31**, 1900065.
8 S. Kumari, D. K. Pradhan, N. R. Pradhan and P. D. Rack, Recent developments on 2D magnetic materials: challenges and opportunities, *Emergent Mater.*, 2021, **4**, 827.
9 P. Joy and S. Vasudevan, Magnetism in the layered transition-metal thiophosphates MPS_3 (M= Mn, Fe, and Ni), *Phys. Rev. B*, 1992, **46**, 5425.
10 A. R. Wildes, S. J. Kennedy and T. J. Hicks, True two-dimensional magnetic ordering in $MnPS_3$, *J. Phys.: Condens. Matter*, 1994, **6**, L335.
11 R. Samal, G. Sanyal, B. Chakraborty and C. S. Rout, Two-dimensional transition metal phosphorous trichalcogenides (MPX3): a review on emerging trends, current state and future perspectives, *J. Mater. Chem. A*, 2021, **9**, 2560.
12 P. Colombet, A. Leblanc, M. Danot and J. Rouxel, Structural aspects and magnetic properties of the lamellar compound $Cu_{0.50}Cr_{0.50}PS_3$, *J. Solid State Chem.*, 1982, **41**, 174.
13 S. Lee, P. Colombet, G. Ouvrard and R. Brec, A new chain compound of vanadium(III): $Ag_{12}V_{12}PS_3$ structure, metal ordering, and magnetic properties, *Mater. Res. Bull.*, 1986, **21**, 917.
14 H. Mutka, C. Payen and P. Molinié, One-Dimensional Heisenberg Antiferromagnet with Spin $S = 3/2$. Experiments on $AgCrP_2S_6$, *Europhys. Lett.*, 1993, **21**, 623.
15 See SI at https://doi.org/10.1039/d5tc03093e for analysis of polarization dependent intensity; temperature-dependent photoluminescence; crystal structure; fitted Raman spectrum; temperature dependent frequency, FWHM, intensity of phonon modes; magnified temperature dependent Raman spectrum; polarization dependence of phonon modes; schematic for polarization configuration; mode visualization, and related tables. The SI also contains ref. 56–67.
16 M. A. Susner, M. Chyasnavichyus, M. A. McGuire, P. Ganesh and P. Maksymovych, Metal Thio- and Selenophosphates as Multifunctional van der Waals Layered Materials, *Adv. Mater.*, 2017, **29**, 1602852.

17 R. Brec, Review on structural and chemical properties of transition metal phosphorous trisulfides MPS_3, *Solid State Ionics*, 1986, **22**, 3.
18 C. Payen, P. Molinie, P. Colombet and G. Fillion, Powder and single crystal susceptibility of the quasi-1D Heisenberg antiferromagnetic chain compounds $AgVP_2S_6$ (S = 1) and $AgCrP_2S_6$ (S = 3/2), *J. Magn. Magn. Mater.*, 1990, **84**, 95.
19 E. Park, J. P. Philbin, H. Chi, J. J. Sanchez, C. Occhialini, G. Varnavides, J. B. Curtis, Z. Song, J. Klein, J. D. Thomsen, M.-G. Han, A. C. Foucher, K. Mosina, D. Kumawat, N. Gonzalez-Yepez, Y. Zhu, Z. Sofer, R. Comin, J. S. Moodera, P. Narang and F. M. Ross, Anisotropic 2D van der Waals Magnets Hosting 1D Spin Chains, *Adv. Mater.*, 2024, **36**, 2401534.
20 K. Kim, S. Y. Lim, J.-U. Lee, S. Lee, T. Y. Kim, K. Park, G. S. Jeon, C.-H. Park, J.-G. Park and H. Cheong, Suppression of magnetic ordering in XXZ-type antiferromagnetic monolayer $NiPS_3$, *Nat. Commun.*, 2019, **10**, 345.
21 M. A. Susner, R. Rao, A. T. Pelton, M. V. McLeod and B. Maruyama, Temperature-dependent Raman scattering and X-ray diffraction study of phase transitions in layered multiferroic $CuCrP_2S_6$, *Phys. Rev. Mater.*, 2020, **4**, 104003.
22 R. Rao, R. Selhorst, B. S. Conner and M. A. Susner, Ferrielectric-paraelectric phase transitions in layered $CuInP_2S_6$ and $CuInP_2S_6$–$In_{4/3}P_2S_6$ heterostructures: a Raman spectroscopy and x-ray diffraction study, *Phys. Rev. Mater.*, 2022, **6**, 045001.
23 V. Kumar, D. Kumar, B. Singh, Y. Shemerliuk, M. Behnami, B. Büchner, S. Aswartham and P. Kumar, Fluctuating fractionalized spins in quasi-two-dimensional magnetic $V_{0.85}PS_3$, *Phys. Rev. B*, 2023, **107**, 094417.
24 B. Singh, D. Kumar, V. Kumar, M. Vogl, S. Wurmehl, S. Aswartham, B. Büchner and P. Kumar, Fractional spin fluctuations and quantum liquid signature in Gd_2ZnIrO_6, *Phys. Rev. B*, 2021, **104**, 134402.
25 X. Wang, Z. Shang, C. Zhang, J. Kang, T. Liu, X. Wang, S. Chen, H. Liu, W. Tang, Y.-J. Zeng, J. Guo, Z. Cheng, L. Liu, D. Pan, S. Tong, B. Wu, Y. Xie, G. Wang, J. Deng, T. Zhai, H.-X. Deng, J. Hong and J. Zhao, Electrical and magnetic anisotropies in van der Waals multiferroic $CuCrP_2S_6$, *Nat. Commun.*, 2023, **14**, 840.
26 P. T. Orban, S. M. Bernier, T. Berry, M. A. Siegler and T. M. McQueen, Random-exchange Heisenberg behavior in the electron-doped quasi-one-dimensional spin-1 chain compound $AgVP_2S_6$, *Phys. Rev. B*, 2024, **110**, 054423.
27 X. Wang, C. Zhu, Y. Deng, R. Duan, J. Chen, Q. Zeng, J. Zhou, Q. Fu, L. You, S. Liu, J. H. Edgar, P. Yu and Z. Liu, van der Waals engineering of ferroelectric heterostructures for long-retention memory, *Nat. Commun.*, 2021, **12**, 1109.
28 Y. Ma, Y. Yan, L. Luo, S. Pazos, C. Zhang, X. Lv, M. Chen, C. Liu, Y. Wang, A. Chen, Y. Li, D. Zheng, R. Lin, H. Algaidi, M. Sun, J. Z. Liu, S. Tu, H. N. Alshareef, C. Gong, M. Lanza, F. Xue and X. Zhang, High-performance van der Waals antiferroelectric $CuCrP_2S_6$-based memristors, *Nat. Commun.*, 2023, **14**, 7891.
29 S. Selter, Y. Shemerliuk, B. Büchner and S. Aswartham, Crystal Growth of the Quasi-2D Quarternary Compound $AgCrP_2S_6$ by Chemical Vapor Transport, *Crystals*, 2021, **11**, 500.
30 G. Kresse and J. Furthmüller, Efficient iterative schemes for ab initio total-energy calculations using a plane-wave basis set, *Phys. Rev. B*, 1996, **54**, 11169.
31 G. Kresse and D. Joubert, From ultrasoft pseudopotentials to the projector augmented-wave method, *Phys. Rev. B*, 1999, **59**, 1758.
32 P. E. Blöchl, Projector augmented-wave method, *Phys. Rev. B*, 1994, **50**, 17953.
33 J. P. Perdew, K. Burke and M. Ernzerhof, Generalized gradient approximation made simple, *Phys. Rev. Lett.*, 1996, **77**, 3865.
34 S. Grimme, J. Antony, S. Ehrlich and H. Krieg, A consistent and accurate ab initio parametrization of density functional dispersion correction (DFT-D) for the 94 elements H-Pu, *J. Chem. Phys.*, 2010, **132**, 154104.
35 A. Togo, L. Chaput, T. Tadano and I. Tanaka, Implementation strategies in phonopy and phono3py, *J. Phys.: Condens. Matter*, 2023, **35**, 353001.
36 A. Togo, First-principles phonon calculations with phonopy and phono3py, *J. Phys. Soc. Jpn.*, 2023, **92**, 012001.
37 D. L. Rousseau, R. P. Bauman and S. P. S. Porto, Normal mode determination in crystals, *J. Raman Spectrosc.*, 1981, **10**, 253.
38 M. Bernasconi, G. Marra, G. Benedek, L. Miglio, M. Jouanne, C. Julien, M. Scagliotti and M. Balkanski, Lattice dynamics of layered MPX_3 (M = Mn, Fe, Ni, Zn; X = S, Se) compounds, *Phys. Rev. B*, 1988, **38**, 12089.
39 M. Balkanski, R. F. Wallis and E. Haro, Anharmonic effects in light scattering due to optical phonons in silicon, *Phys. Rev. B*, 1983, **28**, 1928.
40 D. J. Lockwood and M. G. Cottam, The spin–phonon interaction in FeF_2 and MnF_2 studied by Raman spectroscopy, *J. Appl. Phys.*, 1988, **64**, 5876.
41 A. Ghosh, M. Palit, S. Maity, V. Dwij, S. Rana and S. Datta, Spin–phonon coupling and magnon scattering in few-layer antiferromagnetic $FePS_3$, *Phys. Rev. B*, 2021, **103**, 064431.
42 B. Zhang, Y. Hou, Z. Wang and R. Wu, First-principles studies of spin–phonon coupling in monolayer $Cr_2Ge_2Te_6$, *Phys. Rev. B*, 2019, **100**, 224427.
43 K. Cho, S. Lee, R. Kalaivanan, R. Sankar, K. Y. Choi and S. Park, Tunable ferroelectricity in van der Waals layered antiferroelectric $CuCrP_2S_6$, *Adv. Funct. Mater.*, 2022, **32**, 2204214.
44 M. A. Susner, B. S. Conner, E. Rowe, R. Siebenaller, A. Giordano, M. V. McLeod, C. R. Ebbing, T. J. Bullard, R. Selhorst and T. J. Haugan, Structural, Magnetic, and Optical Properties of the van der Waals Antiferromagnet $AgCrP_2Se_6$, *J. Phys. Chem. C*, 2024, **128**, 4265.
45 I. Zamaraite, A. Dziaugys, J. Banys and Y. Vysochanskii, Dielectric and electrical properties of $AgCrP_2S_6$ and $Cu_{0.2}Ag_{0.8}CrP_2S_6$ layered crystals, *Ferroelectrics*, 2017, **515**, 13.
46 D. Fausti, A. A. Nugroho, P. H. van Loosdrecht, S. A. Klimin, M. N. Popova and L. N. Bezmaternykh, Raman scattering from phonons and magnons in $RFe_3(BO_3)_4$, *Phys. Rev. B*, 2006, **74**, 024403.

47 S. Kamba, Soft-mode spectroscopy of ferroelectrics and multiferroics: a review, *APL Mater.*, 2021, **9**, 020704.
48 J. Tang, B. J. Lawrie, M. Cheng, Y.-C. Wu, H. Zhao, D. Kong, R. Lu, C.-H. Yao, Z. Gai and A.-P. Li, Raman Fingerprints of Phase Transitions and Ferroic Couplings in van der Waals Multiferroic $CuCrP_2S_6$, *J. Phys. Chem. Lett.*, 2025, **16**, 4336.
49 M. Cardona and T. Ruf, Phonon self-energies in semiconductors: anharmonic and isotopic contributions, *Solid State Commun.*, 2001, **117**, 201.
50 B. Singh, G. A. Cansever, T. Dey, A. Maljuk, S. Wurmehl, B. Büchner and P. Kumar, Orbiton–phonon coupling in $Ir^{5+}(5d^4)$ double perovskite Ba_2YIrO_6, *J. Phys.: Condens. Matter*, 2019, **31**, 065603.
51 P. G. Klemens, Anharmonic Decay of Optical Phonons, *Phys. Rev. B*, 1966, **148**, 845.
52 Y. S. Lee, T. W. Noh, J. H. Park, K. B. Lee, G. Cao, J. E. Crow, M. K. Lee, C. B. Eom, E. J. Oh and I.-S. Yang, Temperature-dependent Raman spectroscopy in $BaRuO_3$ systems, *Phys. Rev. B*, 2002, **65**, 235113.
53 J. Scott, Soft-mode spectroscopy: experimental studies of structural phase transitions, *Rev. Mod. Phys.*, 1974, **46**, 83.
54 U. Fano, Effects of configuration interaction on intensities and phase shifts, *Phys. Rev.*, 1961, **124**, 1866.
55 B. Huang, J. Cenker, X. Zhang, E. L. Ray, T. Song, T. Taniguchi, K. Watanabe, M. A. McGuire, D. Xiao and X. Xu, Tuning inelastic light scattering via symmetry control in the two-dimensional magnet CrI_3, *Nat. Nanotechnol.*, 2020, **15**, 212.
56 R. Loudon, The Raman effect in crystals, *Adv. Phys.*, 1964, **13**, 423.
57 J. Kim, J.-U. Lee and H. Cheong, Polarized Raman spectroscopy for studying two-dimensional materials, *J. Phys.: Condens. Matter*, 2020, **32**, 343001.
58 V. Funk, K. Wagner, E. Wietek, J. D. Ziegler, J. Förste, J. Lindlau, M. Förg, K. Watanabe, T. Taniguchi and A. Chernikov, Spectral asymmetry of phonon sideband luminescence in monolayer and bilayer WSe_2, *Phys. Rev. Res.*, 2021, **3**, L042019.
59 A. Boziki, M. I. Dar, G. Jacopin, M. Gratzel and U. Rothlisberger, Molecular origin of the asymmetric photoluminescence spectra of $CsPbBr_3$ at low temperature, *J. Phys. Chem. Lett.*, 2021, **12**, 2699.
60 J. Diouri, J. P. Lascaray and M. E. Amrani, Effect of the magnetic order on the optical-absorption edge in $Cd_{1-x}Mn_xTe$, *Phys. Rev. B*, 1985, **31**, 7995.
61 Y. P. Varshni, Temperature dependence of the energy gap in semiconductors, *Physica*, 1967, **34**, 149.
62 R. Pässler, Basic model relations for temperature dependencies of fundamental energy gaps in semiconductors, *Phys. Status Solidi B*, 1997, **200**, 155.
63 P. Lautenschlager, M. Garriga, S. Logothetidis and M. Cardona, Interband critical points of GaAs and their temperature dependence, *Phys. Rev. B*, 1987, **35**, 9174.
64 C. Yu, Z. Chen, J. J. Wang, W. Pfenninger, N. Vockic, J. T. Kenney and K. Shum, Temperature dependence of the band gap of perovskite semiconductor compound $CsSnI_3$, *J. Appl. Phys.*, 2011, **110**, 063526.
65 S. Wang, J. Ma, W. Li, J. Wang, H. Wang, H. Shen, J. Li, J. Wang, H. Luo and D. Li, Temperature-dependent band gap in two-dimensional perovskites: thermal expansion interaction and electron–phonon interaction, *J. Phys. Chem. Lett.*, 2019, **10**, 2546.
66 S. Rudin, T. Reinecke and B. Segall, Temperature-dependent exciton linewidths in semiconductors, *Phys. Rev. B*, 1990, **42**, 11218.
67 M. Leroux, N. Grandjean, B. Beaumont, G. Nataf, F. Semond, J. Massies and P. Gibart, Temperature quenching of photoluminescence intensities in undoped and doped GaN, *J. Appl. Phys.*, 1999, **86**, 3721.

